ACS Energy LETTERS

http://pubs.acs.org/journal/aelccp

Synthesizing Functional Ceramic Powders for Solid Oxide Cells in Minutes through Thermal Shock

Weiwei Fan,[‖] Zhichu Ren,[‖] Zhu Sun, Xiahui Yao, Bilge Yildiz,* and Ju Li*

Cite This: *ACS Energy Lett.* 2022, 7, 1223−1229

Read Online

ACCESS | Metrics & More | Article Recommendations | Supporting Information

ABSTRACT: Ceramic fuel/electrolysis cells are key energy/material conversion devices. Here, we report that, by thermal shock, mixed ionic and electronic conducting electrode powders with a perovskite structure can be successfully synthesized within 2 min, while this procedure requires a two-step calcination and almost 40 h when a conventional furnace is used. This benefits from the high temperature supplied to the system, greatly enhancing the reaction kinetics among the raw materials. Moreover, typical electrolyte powders with a fluorite structure, such as $(Y_2O_3)_{0.08}(ZrO_2)_{0.92}$ (YSZ) and $Sm_{0.2}Ce_{0.8}O_{1.95}$ (SDC), are also synthesized in several minutes through a thermal shock, which significantly reduces the fabrication time of a solid oxide cell. Also, one can easily prepare multiple samples at one time via tailoring the carbon support size. The availability of fast synthesis of the thermal-shock technique enables the development of new functional ceramic powders for solid-oxide cells in a high-throughput and economical manner.

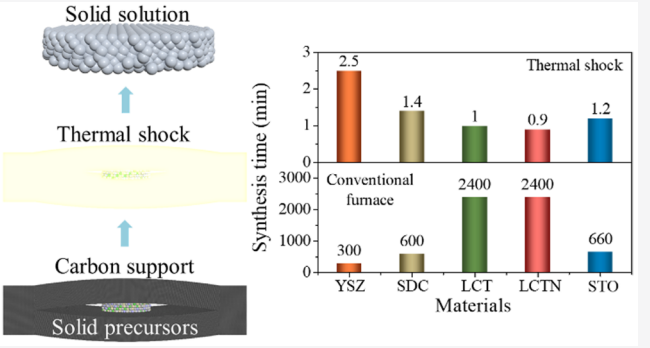

All-solid electrochemical cells are an important class of energy conversion devices,[1−4] benefiting from their high efficiency and environmentally friendly characteristics. They consist of open porous ceramic electrodes and a dense (airtight) ceramic electrolyte membrane.[5] The employed powders are generally prepared by a solid-state reaction (Figure S1) in a furnace.[6,7] Different solids cannot react with each other at room temperature on a normal time scale (Figure 1a). The diffusion length L of a diffusing species is $(2Dt)^{1/2}$, while the diffusion coefficient (D) is temperature (T) dependent ($\propto \exp(-E_a/RT)$); thus, a higher diffusion rate could be expected at a higher temperature. A furnace is conventionally used as the heating source. For furnace-based calcination and/or sintering, generally many hours of treatment is needed to obtain the target phase due to the kinetic limitation (Figure S2).[8−11] Moreover, the heating and cooling rates are low (generally less than 20 °C min^{-1}) due to the thermal inertia of the furnace. Thus, one needs to wait for several to many hours to obtain the target powders.

Extensive efforts have been made in the past to reduce the ceramic synthesis time and cost, such as spark plasma synthesis, microwave synthesis, and flash synthesis. Even though these methods can enhance the reaction kinetics and thus reduce the synthesis time, it is still difficult to experiment with multiple compositions in parallel in a high-throughput way.[12−16] With the aims of rapidly synthesizing and screening multiple functional ceramic powders for solid oxide cells, in this work, a low-cost carbon felt was selected and used as a disposable heating source. To load the as-prepared solid precursors, a cavity was easily manufactured according to the required size of the sample. To increase the contact area of the raw materials and conveniently collect the product(s), the mixtures were compressed into a pellet and then placed into the "mini disposable furnace" surrounded by carbon felt. When a high electronic current was applied across the carbon felt, a large amount of Joule heating can be generated around the sample to drive the solid reaction to take place, thus rapidly forming the target phase (Figure 1b−d). The beauty of this technique includes (1) superhigh heating and cooling rates, (2) flexible size, and (3) low cost. According to the desired dimension of the target sample(s), one can conveniently tailor the size of the carbon

Received: December 2, 2021
Accepted: February 22, 2022

https://doi.org/10.1021/acsenergylett.1c02630
ACS Energy Lett. 2022, 7, 1223−1229

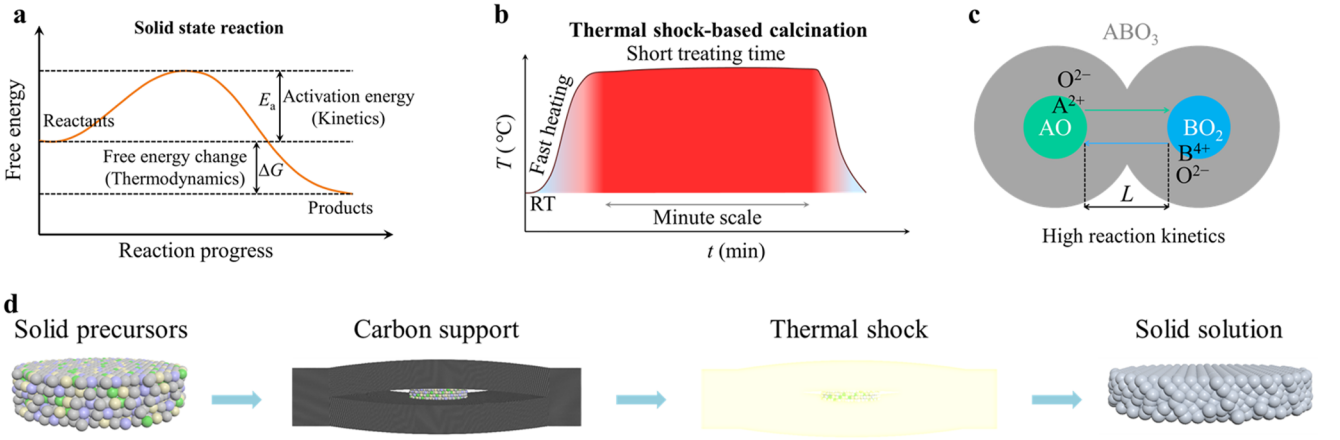

Figure 1. (a) Diagram of the thermodynamics and kinetics of the solid-state reaction. (b) Temperature profile as a function of time for calcining solid precursors using a thermal-shock approach. (c) Illustration of a solid reaction between raw materials. High reaction kinetics can be obtained by thermal shock. (d) Schematic of the fabrication of a solid solution by the thermal-shock technique. Each sphere represents a grain. During thermal shock, a pellet form was adopted to increase the contact area among raw materials and thus to enhance the solid-state reaction kinetics. Also, this was beneficial for the collection of the product.

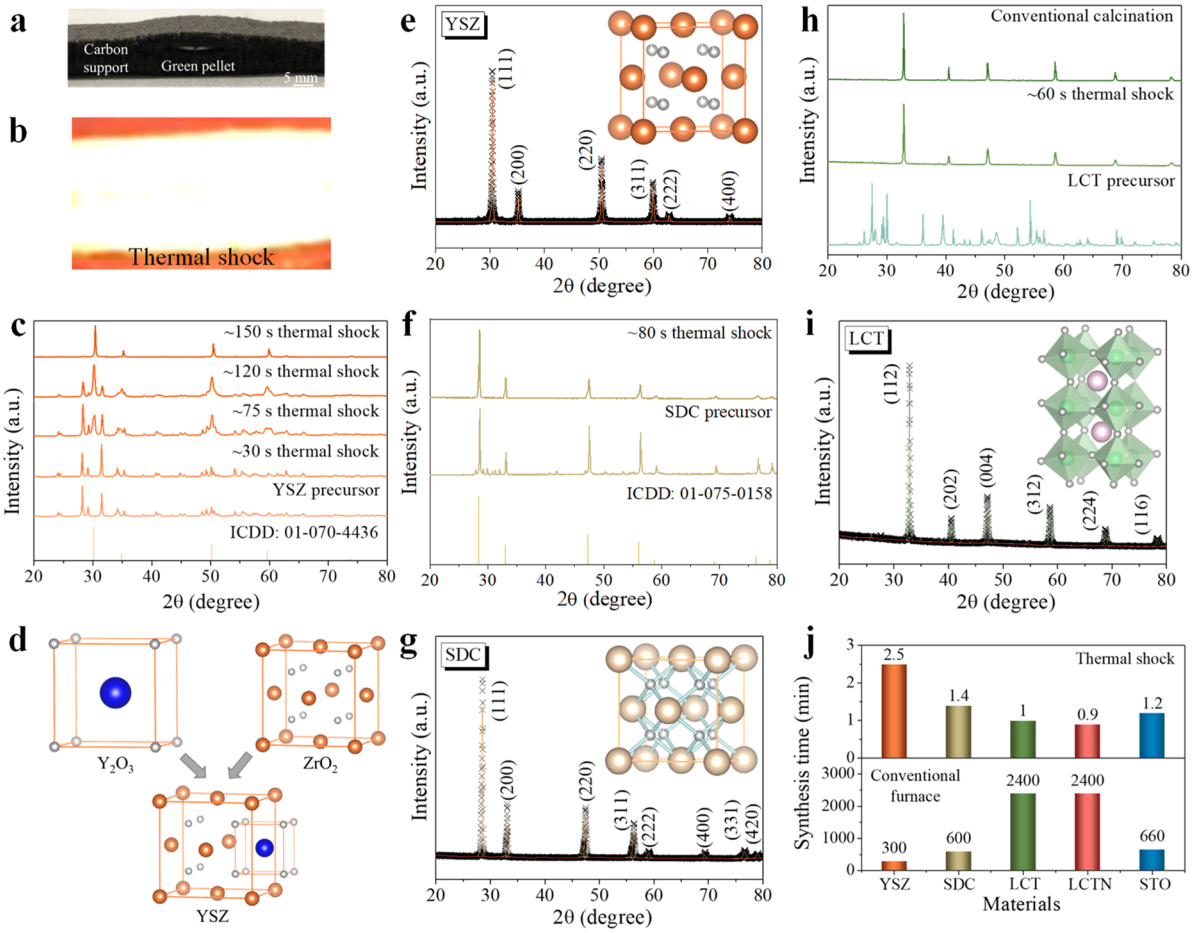

Figure 2. Pictures of the carbon support (a) before and (b) during the thermal shock. (c) XRD profiles of YSZ after thermal shocks for different times. (d) Illustration of the reaction to form YSZ. (e) Rietveld-refined XRD spectrum of the YSZ. The inset shows the crystal structure of YSZ. Orange spheres denote Y/Zr, and gray spheres denote O. (f) XRD profiles of SDC after thermal shocks for different times. (g) Rietveld-refined XRD spectrum of the SDC. The inset shows the crystal structure of SDC. Brown spheres denote Sm/Ce, and gray spheres denote O. (h) XRD profiles of LCT after calcination by thermal shock and a conventional furnace. (i) Rietveld-refined XRD spectrum of LCT. The inset shows the crystal structure of LCT. Pink spheres denote La/Ca, green spheres denote Ti, and gray spheres denote O. (j) Comparison of the synthesis times of ceramic materials by thermal-shock-based and conventional furnace-based approaches.

https://doi.org/10.1021/acsenergylett.1c02630
ACS Energy Lett. 2022, 7, 1223−1229

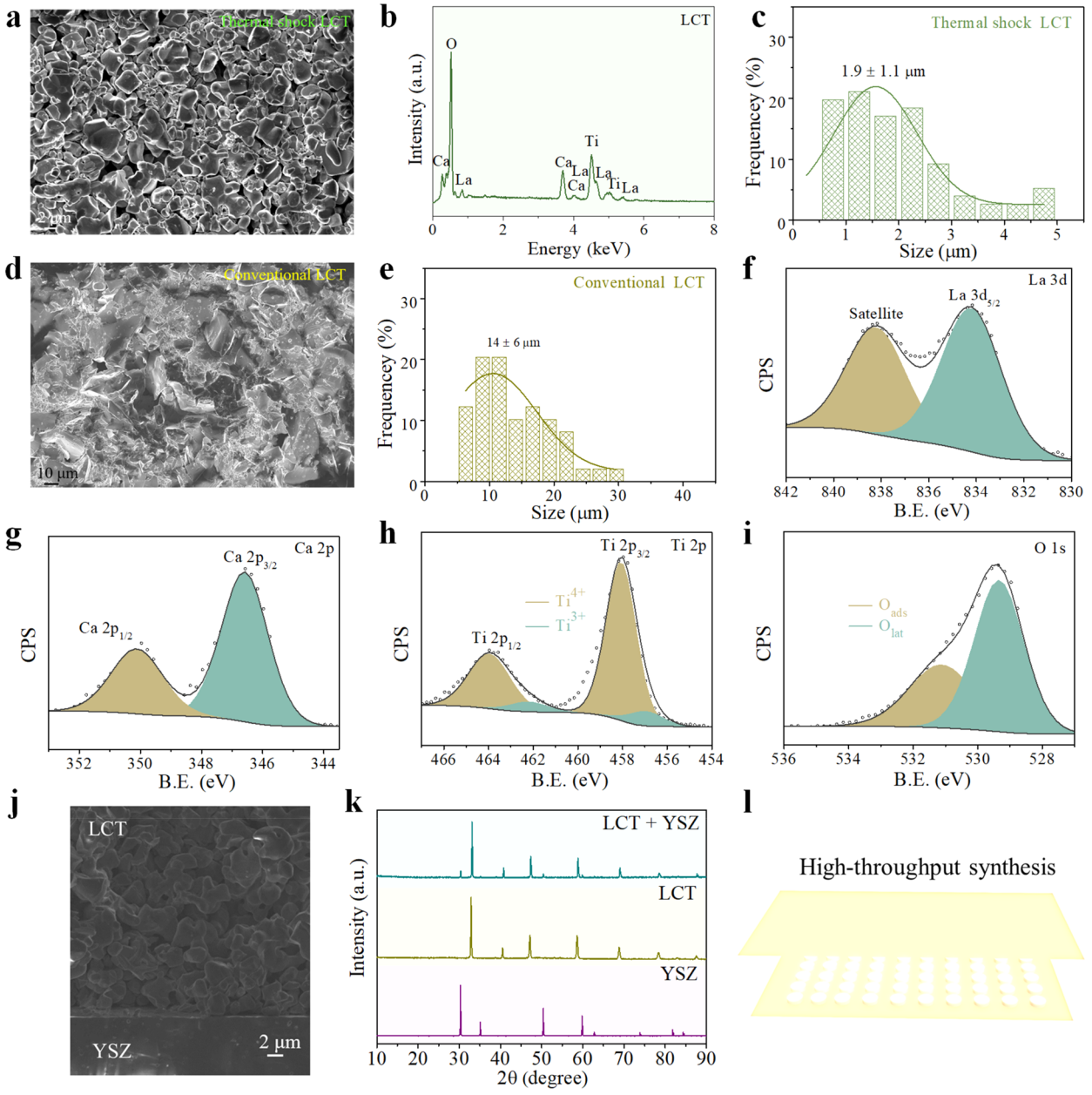

Figure 3. (a) SEM image of the LCT powders after cracking and grinding a pellet with the desired phase synthesized by thermal shock. (b) EDX pattern of LCT synthesized by thermal shock. (c) Particle size distribution of (a). (d) SEM image of the LCT powders after cracking and grinding a pellet fabricated by the conventional method. (e) Particle size distribution of the (d). XPS spectra of (f) La 3d, (g) Ca 2p, (h) Ti 2p, and (i) O 1s of the thermal-shock-synthesized LCT. (j) SEM image of the cross-section view of an LCT electrode printed on a commercial dense YSZ electrolyte. (k) XRD profile of the LCT working electrode on the YSZ electrolyte after sintering at 1200 °C for 3 h. (l) Schematic of the high-throughput synthesis of functional ceramics by the thermal-shock technique.

support. Due to the rapid calcination (usually on a scale of minutes), one can synthesize and screen the functional ceramic powders in a high-throughput manner.

In this work, we showed that a functional ceramic electrode and electrolyte powders with different crystal structures (such as perovskite and fluorite) for solid-oxide cells (SOC) were successfully synthesized within 3 min, while generally, the process requires tens of hours with the conventional furnace-based fabrication. As a demonstration, the thermal-shock-fabricated pellets with the desired phase were also converted into an ink followed by assembly into a solid oxide cell. Subsequently, the electrochemical performance was investigated. Thermal shock opens up a new avenue to rapidly and economically prepare functional ceramic powders for SOCs.

Crystal Structure of the Thermal-Shock-Fabricated SOC Powders. To investigate the feasibility of the rapid synthesis of functional ceramic powders by the thermal-shock technique, we first prepared the $(Y_2O_3)_{0.08}(ZrO_2)_{0.92}$ (YSZ) precursor, which is a popular oxygen-ion conductor material in solid oxide cells. Subsequently, the as-prepared sample was sandwiched in the carbon support followed by a thermal shock (Figure 2a,b). The results showed that no obvious change occurred in the XRD profile after thermal shock for ~30 s (Figure 2c), suggesting that nearly no reaction took place among the raw materials during the calcination. A change was observed

https://doi.org/10.1021/acsenergylett.1c02630
ACS Energy Lett. 2022, 7, 1223−1229

in the XRD profile after thermal shock for ~75 s, implying a partial solid-state reaction took place and more calcination time was needed to acquire the desired phase. As expected, with the increase of shock time to ~120 s, the extent of the solid reaction proceeded further, and the main phase appeared. Surprisingly, after a thermal shock of around 150 s, a single phase was acquired, suggesting that the yttrium was incorporated into the lattice (Figure 2d) and a solid-solution oxide was formed during the thermal shock. Using a conventional furnace, generally several hours are required to obtain the YSZ product.[17] In addition, the results showed that the as-synthesized YSZ could be well indexed on the basis of a cubic fluorite structure belonging to the space group $Fm\bar{3}m$ (No. 225) (Figure 2e), and the lattice parameter was $a = b = c = 5.1411(1)$ Å (Table S1). To further investigate the feasibility of synthesizing the fluorite structure ceramic by the thermal-shock approach, subsequently, the precursor of $Sm_{0.2}Ce_{0.8}O_{1.95}$ (SDC), another broadly used Ce-based ionic conductor in solid oxide cells,[18] was prepared. It was found that after a thermal shock of ~80 s, a single SDC phase was acquired (Figure 2f,g and Table S2). Thus, the fabrication period of SDC-based solid oxide cells can be significantly reduced by the thermal-shock technique.

On consideration that the perovskite oxides, which generally need tens of hours to synthesize by a conventional furnace, are good candidates for solid-oxide cells due to the mixed ionic and electronic conducting (MIEC) properties, the Ti-based oxide $La_{0.4}Ca_{0.4}TiO_{3-\delta}$ (LCT) was subsequently investigated. It was found that a solid solution was formed after a thermal shock of ~60 s (Figure 2h). Moreover, the results showed that the as-synthesized LCT presented a perovskite orthorhombic structure belonging to space group *Pbnm* (No. 62) (Figure 2i and Table S3). The LCT crystal structure can be represented by a 3D network of BO_6 octahedra filled with the A-site cations among them. For comparison, an LCT precursor was also calcined in a conventional furnace; a single perovskite phase was acquired after treatment for ~40 h.

Generally, for perovskite oxides, the introduction of another transition metal possessing lower valence and superb catalytic activity can tune the electrochemical properties of the host oxide; therefore, nickel was introduced and the $La_{0.4}Ca_{0.4}Ti_{0.94}Ni_{0.06}O_{3-\delta}$ (LCTN) precursor was thermally shocked for different times. Similarly, the results showed that with an increase of shock time (Figure S3), the reaction took place and the primary phase formed after an ~30 s shock. After a thermal shock of around 55 s, a perovskite phase was achieved (Table S4). In addition, the cubic structure $SrTiO_3$ (STO, a good candidate for an electrode backbone for infiltration) within space group $Pm\bar{3}m$ (No. 221) was also successfully synthesized after thermal shock for ~70 s (Figure S4 and Tables S5 and S6). By comparison, it was found that the functional ceramic oxides generally can be synthesized in several minutes by a thermal shock (Figure 2j), while these oxides require several or tens of hours with the traditional furnace-based approach,[17−19] indicating that the thermal-shock technique can greatly enhance the solid reaction kinetics. The fast synthesis ability of this technique can not only greatly decrease the fabrication cost and time of electrode and electrolyte powders for solid oxide cells but also facilitate the development of more advanced ceramics.

Microstructural and Chemical States of the Thermal Shock Fabricated Powders. To investigate the micromorphology, chemical states, and electrochemical performance of the thermal-shock-synthesized ceramics, the pellet products with the desired phase were cracked and ground into powders. Subsequently, scanning electron microscopy (SEM) was carried out. It was observed that the LCT powder surfaces showed a terrace-like microstructure (Figure 3a and Figure S5), which is typical for an A-site-deficient perovskite oxide.[11] The energy-dispersive X-ray (EDX) result confirmed the composition of La, Ca, Ti, and O elements (Figure 3b). Moreover, an average particle size of 1.9 ± 1.1 μm was obtained for the thermal-shock-fabricated LCT powders (Figure 3c). For comparison, conventional furnace-prepared LCT was also investigated. Due to the long-term treatment, a coarsening phenomenon was very severe, resulting in a denser electrode (Figure 3d and Figure S6). The average particle size is 14 ± 6 μm (Figure 3d). Similarly, our YSZ product showed a particle size of ~500 nm (Figure S7), which is relatively smaller than that of the product prepared by a conventional furnace (usually micrometer size). This is mainly due to the short treatment time (several minutes), limiting the particle coarsening after solid-state synthesis. In other words, one can easily acquire functional ceramic powders with a smaller particle size through the rapid synthesis technique of thermal shock. Small particle sizes are often beneficial for ceramic electrochemical cells due to better fracture toughness and thermal quench-cracking resistance. Additionally, EDX results also confirmed the corresponding compositions of SDC, STO, and LCTN powders (Figures S8−S11).

To verify the chemical states of the synthesized powders, X-ray photoelectron spectroscopy (XPS) was conducted on the samples. The C 1s peak (284.8 eV) was used as a reference to calibrate all the collected spectra, and a Shirley-type background was employed during fitting.[20] For LCT, the survey scan XPS result further revealed the composition of La, Ca, Ti, and O elements (Figure S12). Figure 3f shows the La 3d core spectrum of LCT, associated with La^{3+} in a perovskite lattice.[21] Similarly, the main peaks appearing in the Ca 2p spectrum (Figure 3g) correspond to the Ca^{2+} in LCT.[22] With regard to the Ti 2p core spectrum,[23] it presents a double excitation. The peaks appearing at 464 eV for Ti $2p_{1/2}$ and 458.1 eV for Ti $2p_{3/2}$ can be attributed to Ti^{4+}, while the peaks located at 462.2 eV for Ti $2p_{1/2}$ and 456.9 eV for Ti $2p_{3/2}$ can be attributed to Ti^{3+} (Figure 3h). For O 1s (Figure 3i), it could be fitted into two subpeaks. The peak with a lower binding energy of 529.4 eV was related to the structure O^{2-}, whereas the peak at 531.2 eV was attributed to the adsorbed oxygen from the ambient atmosphere.[24] In addition, for YSZ, the core spectra of Y 3d, Zr 3d, and O 1s further suggested the composition of the lattice Y^{3+}, Zr^{4+}, and O^{2-} (Figure S13).

For use in solid oxide cells, the electrode powders should have good compatibility with the electrolyte. Therefore, to investigate the chemical and thermal compatibility of the thermal-shock-fabricated electrode powders with the standard commercial YSZ electrolyte, the as-prepared powders were converted into an ink with the proper viscosity and printed on the surface of the YSZ, followed by heterophase diffusion bonding at 1200 °C for 3 h. The result showed that there was a good adhesion between our LCT porous electrode and the commercial YSZ dense electrolyte membrane, and no delamination was observed (Figure 3j). Moreover, the XRD result showed that no obvious additional peaks formed after the diffusion bonding (Figure 3k), implying a desirable chemical compatibility of the thermal-shock-fabricated electrode powders with the YSZ electrolyte. Due to the rapid synthesis ability of the thermal-shock technique, one can prepare and screen new ceramic powders in a high-throughput way. Multiple samples of different compositions can be synthesized in parallel by tailoring the

https://doi.org/10.1021/acsenergylett.1c02630
ACS Energy Lett. 2022, 7, 1223−1229

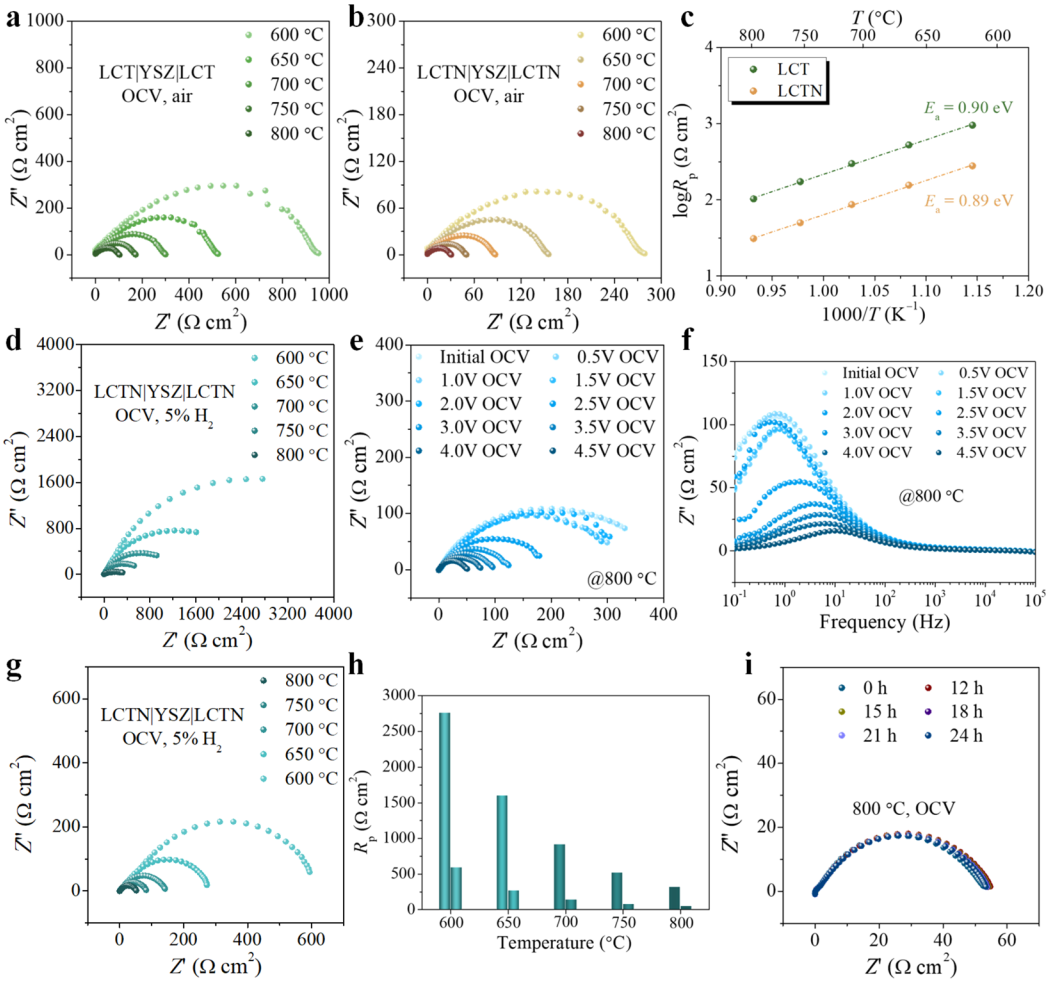

Figure 4. Nyquist plots of (a) LCT|YSZ|LCT and (b) LCTN|YSZ|LCTN symmetrical cells collected from 600 to 800 °C in air under OCV conditions. (c) Arrhenius plots of R_p for LCT and LCTN electrodes in air. (d) Nyquist plots of an LCTN|YSZ|LCTN symmetrical cell collected from 600 to 800 °C under a wet (3% H_2O) 5% H_2/95% N_2 atmosphere under OCV conditions. (e) Nyquist and (f) Bode plots of LCTN collected under OCV conditions after voltage shock at different voltages at 800 °C under a wet (3% H_2O) 5% H_2/95% N_2 atmosphere. (g) Nyquist plots of LCTN collected from 800 to 600 °C in wet (3% H_2O) 5% H_2/95% N_2 under OCV conditions after a voltage shock at 800 °C. (h) Comparison of R_p values of LCTN at different temperatures in wet (3% H_2O) 5% H_2/95% N_2 after voltage shock. (i) R_p collected at different times at 800 °C after a voltage shock.

carbon support to the desired size (Figure 3l and Figures S14 and S15). In this mode, the efficiency of developing new functional materials can be greatly enhanced, facilitating the discovery of new advanced ceramics for electrochemical energy devices.

Electrochemical Performance of the Thermal-Shock-Synthesized Powders. To investigate the electrochemical performance of the electrode powders of solid oxide cells, usually a symmetrical configuration is applied to benchmark their electrocatalytic activity.[25] On consideration of the desirable thermal and chemical compatibility between YSZ and LCT and LCTN (Figure S16), commercial YSZ electrolyte supported symmetrical cells were prepared and tested under open-circuit voltage (OCV) conditions using a homemade setup (Figure S17).

As shown in Figure 4a, with an increase in the temperature from 600 to 800 °C, the polarization resistance (R_p) of the thermal-shock-synthesized LCT perovskite decreased from 954 to 103 Ω cm^2 in air, attributed to the thermal activation of the electrochemical reactions. For comparison, the electrochemical performance of the conventional-furnace-synthesized LCT (Figure S18) was also investigated under the same conditions. The results showed that larger R_p values were obtained (Figure S19), suggesting an inferior electrocatalytic activity for the oxygen reduction reaction (ORR). This improved performance of the rapidly synthesized electrode powders is presumably related to the small particle size obtained by thermal shock, which can increase the gas diffusion area and shorten the transport path, thus accelerating the electrochemical reactions occurring on the electrode. Subsequently, the electrochemical impedance spectra (EIS) of the thermal-shock-synthesized LCTN electrode powders were collected. It was found that the R_p values varied between 279 and 31 Ω cm^2 in air during the measurement (Figure 4b), which were much lower than that of LCT. This was mainly due to the fact that, when an element with lower valence state was introduced at the B site of the perovskite oxide, to maintain the charge neutrality additional oxygen vacancies will be formed in the perovskite lattice, facilitating the migration of the oxygen ions. Moreover, a lower activation energy (E_a) was obtained for the LCTN perovskite (Figure 4c), verifying the enhanced electrochemical kinetics for the ORR. In addition, further improved electrocatalytic activity was obtained

https://doi.org/10.1021/acsenergylett.1c02630
ACS Energy Lett. 2022, 7, 1223−1229

by using a LCTN:YSZ (50:50) composite as the electrode (Figure S20), ascribed to the increased concentration of oxygen vacancies and an extended three-phase boundary length for oxygen ion transfer.

To obtain more information about the electrochemical performance of the LCTN perovskite electrode, wet (3% H_2O) 5% H_2/95% N_2 was introduced into the chamber, and then EIS was collected after stabilization. Results showed that the R_p value went from 2762 to 324 Ω cm^2 in the temperature range of 600−800 °C (Figure 4d). In comparison to those in air, larger R_p values were acquired in a reducing atmosphere. This can most probably be ascribed to the p-type conducting behavior of the LCTN (Figure S21). To improve the electrocatalytic activity of the LCTN perovskite oxide, an external voltage was applied to trigger the exsolution of nanoparticles with superb catalytic activity from the perovskite lattice. As shown in Figure 4e, R_p changed slightly after voltage shock before 1.5 V at 800 °C. In the range of 2−4 V, R_p gradually decreased from 179 to 74 Ω cm^2. At 4.5 V, the R_p value reached 50 Ω cm^2; an almost 6-fold enhancement was obtained in comparison to the R_p of LCTN before the voltage shock, suggesting that the electrocatalytic activity of LCTN was improved greatly. This was mainly due to the exsolved nanoparticles, which could provide sufficient active sites for the electrochemical oxidation of hydrogen, such as hydrogen adsorption ($H_2 \leftrightarrow 2H_{ads}$), dissociation ($H \leftrightarrow H^+ + e^-$), and water formation ($2H^+ + O^{2-} \leftrightarrow H_2O$). Moreover, the results showed that, during the voltage shock, the impedance change primarily came from the low-frequency portion (Figure 4f), suggesting that the enhancement of the electrochemical kinetics is associated with the gas adsorption and dissociation processes.

To further investigate the electrocatalytic activity of LCTN after the voltage shock, the temperature was decreased programmatically to 600 °C. It was found that the R_p value increased from 50 to 594 Ω cm^2 with a decrease in the environmental temperature (Figure 4g). In comparison to those before the voltage shock, the R_p values were still promising at lower temperatures after the voltage shock (Figure 4h), further demonstrating that the electrocatalytic activity of LCTN was enhanced. In addition, no obvious change in R_p was detected during the measurement (Figure 4i), indicating a favorable stability of the product. Overall, one can rapidly synthesize the perovskite electrode powders by a thermal shock as well as tune the electrocatalytic activity through an electrochemical voltage shock, greatly enhancing the flexibility of the advanced ceramics in the application of electrochemical cells.

In summary, by rapid Joule heating by a thermal shock inside carbon felt, oxide electrode powders with a perovskite structure for solid-oxide cells can generally be synthesized in 2 min. In contrast, it usually takes tens of hours to acquire the desired phase by using a conventional furnace. This is mainly due to the remarkably enhanced reaction kinetics among the precursors during the thermal shock. We report that other popular electrolyte powders with a fluorite structure, i.e. YSZ and SDC, can also be synthesized in minutes by a thermal shock, implying that the fabrication time and the cost of electrode and electrolyte powders for solid-oxide cells can be greatly reduced. We also report that the thermal-shock-synthesized powders show reasonable electrochemical performance, which can be further improved by an *in situ* electrochemical voltage shock. The rapid synthesis ability of the thermal-shock approach facilitates the discovery of new functional ceramics in a high-throughput manner.

■ ASSOCIATED CONTENT

Supporting Information

The Supporting Information is available free of charge at https://pubs.acs.org/doi/10.1021/acsenergylett.1c02630.

Experimental details, schematic of the solid-state reaction, XRD profiles, SEM images, EDX pattern, XPS spectrum, Nyquist plots, conductivity, Rietveld refined parameters, and thermal shock parameters (PDF)

■ AUTHOR INFORMATION

Corresponding Authors

Bilge Yildiz − *Department of Nuclear Science and Engineering and Department of Materials Science and Engineering, Massachusetts Institute of Technology, Cambridge, Massachusetts 02139, United States;* orcid.org/0000-0002-2688-5666; Email: byildiz@mit.edu

Ju Li − *Department of Nuclear Science and Engineering and Department of Materials Science and Engineering, Massachusetts Institute of Technology, Cambridge, Massachusetts 02139, United States;* orcid.org/0000-0002-7841-8058; Email: liju@mit.edu

Authors

Weiwei Fan − *Department of Nuclear Science and Engineering, Massachusetts Institute of Technology, Cambridge, Massachusetts 02139, United States;* orcid.org/0000-0001-6298-8964

Zhichu Ren − *Department of Materials Science and Engineering, Massachusetts Institute of Technology, Cambridge, Massachusetts 02139, United States*

Zhu Sun − *State Key Laboratory of Electrical Insulation and Power Equipment, Xi'an Jiaotong University, Xi'an 710049, People's Republic of China*

Xiahui Yao − *Department of Nuclear Science and Engineering, Massachusetts Institute of Technology, Cambridge, Massachusetts 02139, United States*

Complete contact information is available at: https://pubs.acs.org/10.1021/acsenergylett.1c02630

Author Contributions

‖W.F. and Z.R. contributed equally to this work.

Notes

The authors declare no competing financial interest.

■ ACKNOWLEDGMENTS

This work was funded by LCEC MATERIALS SEED, grants number 2565243. J.L. acknowledges support by the Department of Energy, Basic Energy Sciences, under award number DE-SC0002633 (Chemomechanics of Far-From-Equilibrium Interfaces).

■ REFERENCES

(1) Zhang, Y.; et al. Thermal-expansion offset for high-performance fuel cell cathodes. *Nature* **2021**, *591*, 246−251.

(2) Shao, Z. P.; Haile, S. M. A high-performance cathode for the next generation of solid-oxide fuel cells. *Nature* **2004**, *431*, 170−173.

(3) Wachsman, E. D.; Lee, K. T. Lowering the temperature of solid oxide fuel cells. *Science* **2011**, *334*, 935−939.

(4) Papac, M.; Stevanovi, V.; Zakutayev, A.; O'Hayre, R. Triple ionic-electronic conducting oxides for next-generation electrochemical devices. *Nat. Mater.* **2021**, *20*, 301−313.

(5) Boldrin, P.; Brandon, N. P. Progress and outlook for solid oxide fuel cells for transportation applications. *Nature Catalysis* **2019**, *2*, 571−577.
(6) Myung, J. H.; Neagu, D.; Miller, D. N.; Irvine, J. T. S. Switching on electrocatalytic activity in solid oxide cells. *Nature* **2016**, *537*, 528−531.
(7) Neagu, D.; et al. Nano-socketed nickel particles with enhanced coking resistance grown in situ by redox exsolution. *Nat. Commun.* **2015**, *6*, 1−8.
(8) Huang, Y. H.; Dass, R. I.; Xing, Z. L.; Goodenough, J. B. Double perovskites as anode materials for solid-oxide fuel cells. *Science* **2006**, *312*, 254−257.
(9) Neagu, D.; Tsekouras, G.; Miller, D. N.; Menard, H.; Irvine, J. T. S. In situ growth of nanoparticles through control of non-stoichiometry. *Nat. Chem.* **2013**, *5*, 916−923.
(10) Tsekouras, G.; Neagu, D.; Irvine, J. T. S. Step-change in high temperature steam electrolysis performance of perovskite oxide cathodes with exsolution of B-site dopants. *Energy Environ. Sci.* **2013**, *6*, 256−266.
(11) Fan, W. W.; Sun, Z.; Bai, Y.; Wu, K.; Cheng, Y. H. Highly stable and efficient perovskite ferrite electrode for symmetrical solid oxide fuel cells. *ACS Appl. Mater. Interfaces* **2019**, *11*, 23168−23179.
(12) Mishra, R. R.; Sharma, A. K. Microwave-material interaction phenomena: Heating mechanisms, challenges and opportunities in material processing. *Composites Part a-Applied Science and Manufacturing* **2016**, *81*, 78−97.
(13) Oghbaei, M.; Mirzaee, O. Microwave versus conventional sintering: A review of fundamentals, advantages and applications. *J. Alloys Compd.* **2010**, *494*, 175−189.
(14) Guillon, O.; et al. Field-assisted sintering technology/spark plasma sintering: Mechanisms, materials, and technology developments. *Adv. Eng. Mater.* **2014**, *16*, 830−849.
(15) Zhang, Y. Y.; Nie, J. Y.; Chan, J. M.; Luo, J. Probing the densification mechanisms during flash sintering of ZnO. *Acta Mater.* **2017**, *125*, 465−475.
(16) Wang, C. W.; et al. A general method to synthesize and sinter bulk ceramics in seconds. *Science* **2020**, *368*, 521−526.
(17) Zarkov, A.; et al. On the synthesis of yttria-stabilized zirconia: a comparative study. *J. Sol-Gel Sci. Technol.* **2015**, *76*, 309−319.
(18) Fan, W. W.; Sun, Z.; Zhou, J.; Wu, K.; Cheng, Y. H. Characterization of Sr/Ru co-doped ferrite based perovskite as a symmetrical electrode material for solid oxide fuel cells. *J. Power Sources* **2017**, *348*, 94−106.
(19) Yamaguchi, Y.; et al. Efficient photocatalytic degradation of gaseous acetaldehyde over ground Rh-Sb co-doped $SrTiO_3$ under visible light irradiation. *Rsc Advances* **2018**, *8*, 5331−5337.
(20) Fan, W. W.; et al. A new family of Ce-doped $SmFeO_3$ perovskite for application in symmetrical solid oxide fuel cells. *J. Power Sources* **2016**, *312*, 223−233.
(21) Uma, M.; et al. Structural, chemical and electrical properties of Au/La_2O_3/n-GaN MIS junction with a high-k lanthanum oxide insulating layer. *J. Electron. Mater.* **2019**, *48*, 4217−4225.
(22) Liu, Q.; Li, J. G.; Zhou, Z. Z.; Xie, J. P.; Lee, J. Y. Hydrophilic mineral coating of membrane substrate for reducing internal concentration polarization (ICP) in forward osmosis. *Sci. Rep.* **2016**, *6*, 1−10.
(23) Yang, L. M.; et al. Redox-reversible niobium-doped strontium titanate decorated with in situ grown nickel nanocatalyst for high-temperature direct steam electrolysis. *Dalton Transactions* **2014**, *43*, 14147−14157.
(24) Ghaffari, M.; Shannon, M.; Hui, H.; Tan, O. K.; Irannejad, A. Preparation, surface state and band structure studies of $SrTi_{(1-x)}Fe_{(x)}O_{(3-\delta)}$ (x = 0−1) perovskite-type nano structure by X-ray and ultraviolet photoelectron spectroscopy. *Surf. Sci.* **2012**, *606*, 670−677.
(25) Choi, Y.; et al. Unravelling inherent electrocatalysis of mixed-conducting oxide activated by metal nanoparticle for fuel cell electrodes. *Nat. Nanotechnol.* **2019**, *14*, 245−251.

https://doi.org/10.1021/acsenergylett.1c02630
ACS Energy Lett. 2022, 7, 1223−1229

Synthesizing functional ceramic powders for solid oxide cells in minutes through thermal shock

Weiwei Fan[1,#] Zhichu Ren[1,#] Zhu Sun[3], Xiahui Yao[1], Bilge Yildiz[1,2*] and Ju Li[1,2*]

[1]Department of Nuclear Science and Engineering, Massachusetts Institute of Technology, Cambridge, MA 02139, USA.

[2]Department of Materials Science and Engineering, Massachusetts Institute of Technology, Cambridge, MA 02139, USA.

[3]State Key Laboratory of Electrical Insulation and Power Equipment, Xi'an Jiaotong University, Xi'an 710049, People's Republic of China

[#]W.W.F. and Z.C.R. contributed equally to this work.

*Corresponding author emails: liju@mit.edu; byildiz@mit.edu

Materials and methods

For preparing the precursors, the corresponding raw materials were weighed carefully using a Mettler Toledo precise balance. ZrO_2 (99%, Sigma Aldrich) and Y_2O_3 (99.99%, Sigma Aldrich) powders were used for preparing $(ZrO_2)_{0.92}(Y_2O_3)_{0.08}$ (YSZ) precursor; Sm_2O_3 (99.9%, Sigma Aldrich) and CeO_2 (99.9%, Sigma Aldrich) powders were used for preparing $Sm_{0.2}Ce_{0.8}O_{1.95}$ (SDC) precursor; La_2O_3 (99.999%, Sigma Aldrich), $CaCO_3$ (99.999%, Alfa), TiO_2 (99.98%, Sigma Aldrich) and NiO (99.99%, Sigma Aldrich) powders were used for preparing $La_{0.4}Ca_{0.4}TiO_{3-\delta}$ (LCT) and $La_{0.4}Ca_{0.4}Ti_{0.94}Ni_{0.06}O_{3-\delta}$ (LCTN) precursors; $SrCO_3$ (99.9%, Sigma Aldrich) and TiO_2 (99.98%, Sigma Aldrich) powders were used for preparing $SrTiO_3$ (STO) precursor, respectively. Subsequently, the powders were fully mixed by a ball miller using zirconia balls. Ethanol was used as the media during milling. The powders were collected after evaporating the ethanol on a digital hot plate, and compressed into pellets by a hydraulic press with 10 mm diameter under the pressure of 5 ton and dwelling for ~15 min. Regarding the preparation of LCT and LCTN by conventional furnace, the corresponding precursors were calcined in two steps. Firstly, they were calcined at 1100 ℃ for 20 h and then fully ball milled. Secondly, they were calcined at 1350 ℃ for 20 h to acquire the desired phase.

Carbon felt (Fuel Cell Store) was used as the support. Before the thermal shock, the as-prepared pellet was sandwiched in the carbon support, which was fixed in the home-made setup coupled with a programmable power supply (VOLTEQ HY5020EP, 0-20A, 0-50V) with maximum power of 1000 W.

Cell fabrication

To prepare the symmetrical cells, the as-prepared pellets with desired phases were firstly cracked and ground. Subsequently, the collected powders were fully dispersed into the ink vehicle (Fuel Cell Materials) by Thinky stirrer to prepare the electrode ink with proper viscosity. The slurry was then symmetrically printed on both sides of the commercial YSZ (Fuel Cell Materials) electrolyte (~140 μm thickness) through customized masks and followed by heating at 1200 ℃ for 3 h in a furnace to get the working electrodes.

Characterization

PANalytical XPert and AERIS X-ray diffractometers (XRD, Cu Kα radiation) were applied to investigate the crystal structure of the materials synthesized by thermal shock. HighScore Plus software was employed to refine the obtained XRD profiles. Zeiss Merlin scanning electron microscopy (SEM) coupled with an energy-dispersive

X-ray detector (EDS) was employed to collect the microstructure information of the synthesized materials. Conductivity was measured from 500 to 800 ℃ in air and 5%H_2 atmospheres by Keithley 2450. PARSTAT 4000 analyzer (Princeton Applied Research) was applied to monitor the electrochemical impedance spectra (EIS) in the frequency range of 10^5−10^{-1} Hz under an AC amplitude of 10 mV.

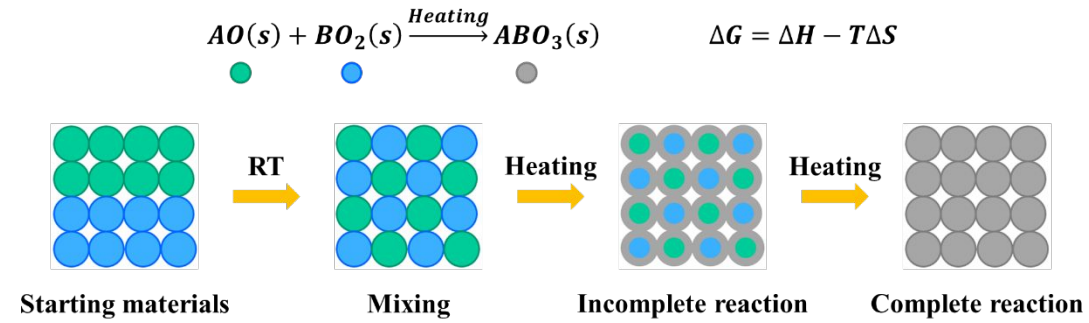

Figure S1. Schematic of formation of new solid product through solid-state reaction method.

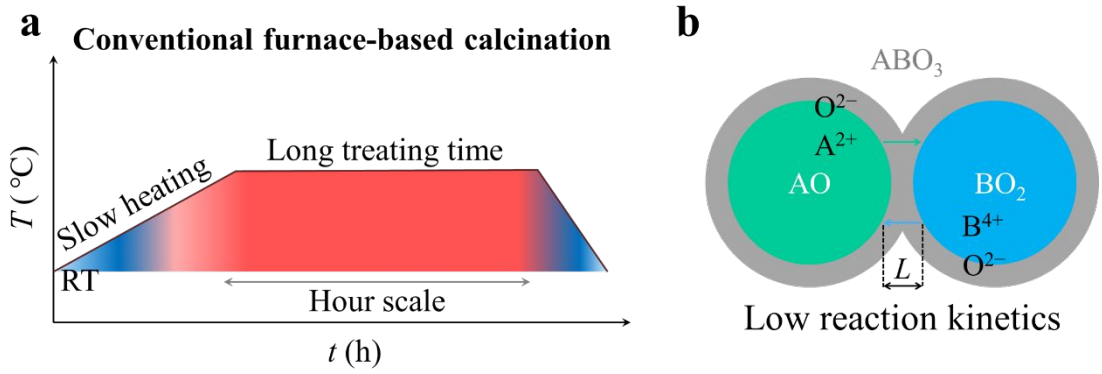

Figure S2. **a,** Temperature profile as a function of time for calcining solid precursors using convention furnace. **b,** Illustration of solid reaction between raw materials. Due to the low driving force provided by the conventional furnace, the reaction kinetics are slow.

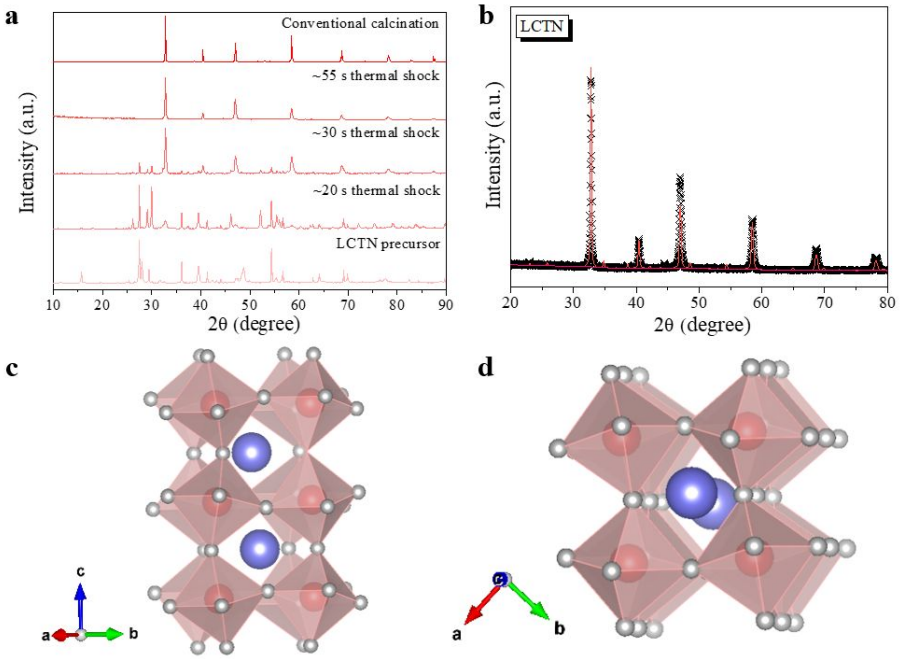

Figure S3. **a,** XRD profiles of LCTN after thermal shock for different time. **b,** Rietveld-refined XRD spectrum of the thermal shock synthesized LCTN. **c, d,** Crystal structure of LCTN at different direction views. Light Blue sphere represents La/Ca, red sphere represents Ti/Ni, grey sphere represents O.

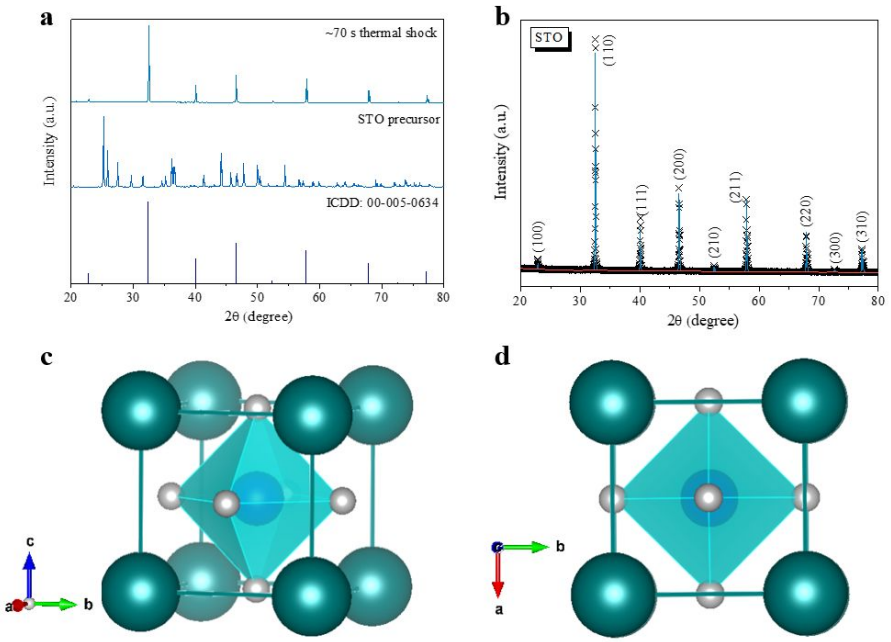

Figure S4. **a,** XRD profiles of STO precursor and after thermal shock for ~70 s. X-ray peaks of STO (ICDD: 00-005-0634) is also shown. **b,** Rietveld-refined XRD spectrum of the thermal shock synthesized STO. **c, d,** Crystal structure of STO at different direction views. Blue sphere represents Ti, grey sphere represents O, dark green represents Sr.

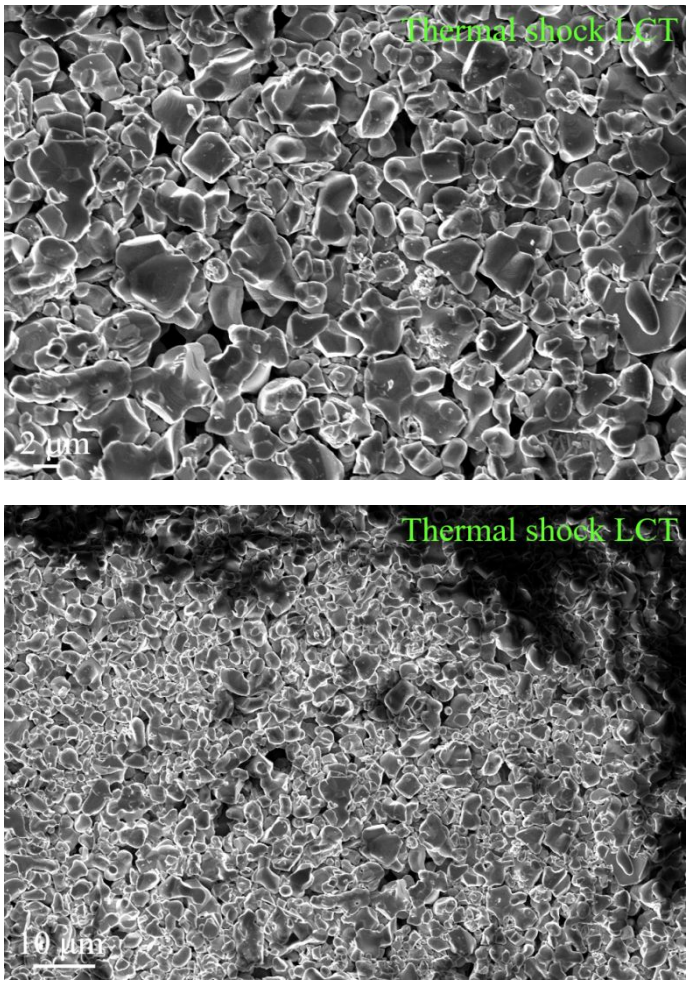

Figure S5. SEM images of the thermal shock synthesized LCT powders.

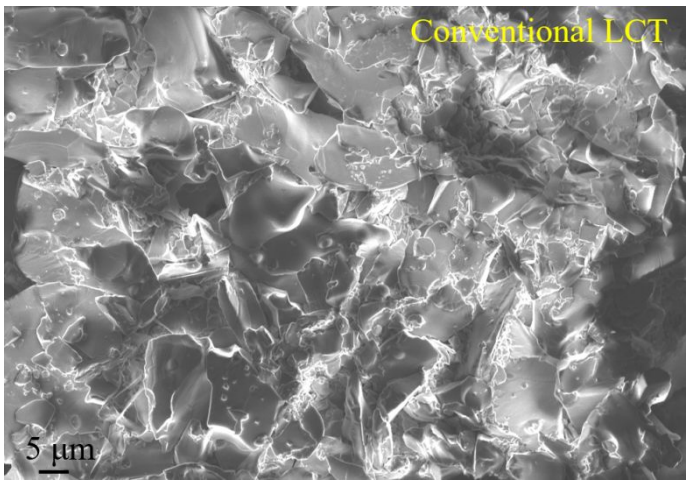

Figure S6. SEM images of the conventional synthesized LCT powders.

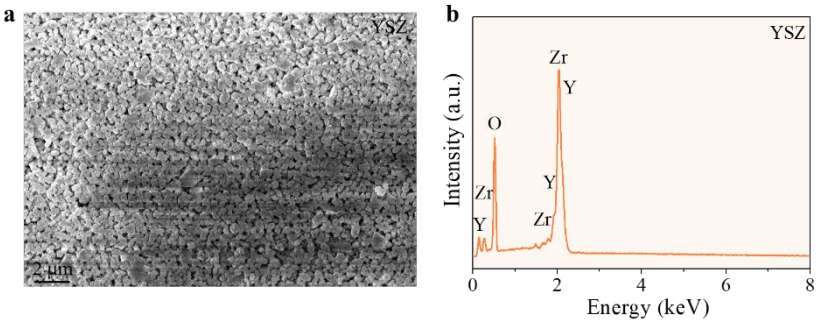

Figure S7. **a,** SEM image of YSZ. **b,** EDX pattern of YSZ.

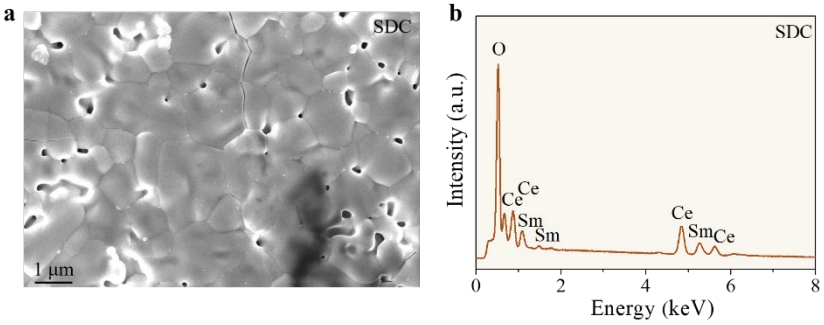

Figure S8. **a,** SEM image of SDC. **b,** EDX pattern of SDC.

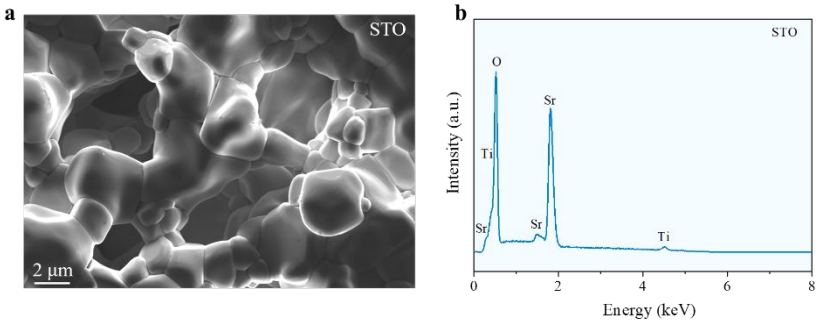

Figure S9. **a,** SEM image of STO. **b,** EDX pattern of STO.

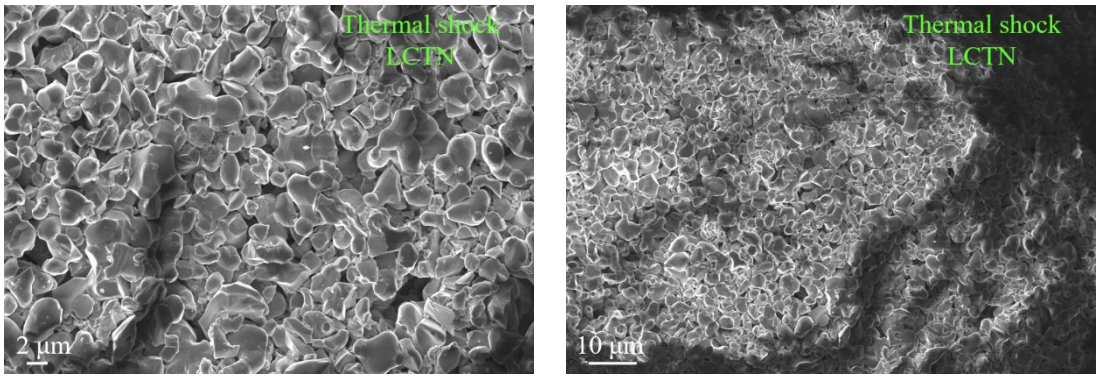

Figure S10. SEM images of the thermal shock synthesized LCTN powders.

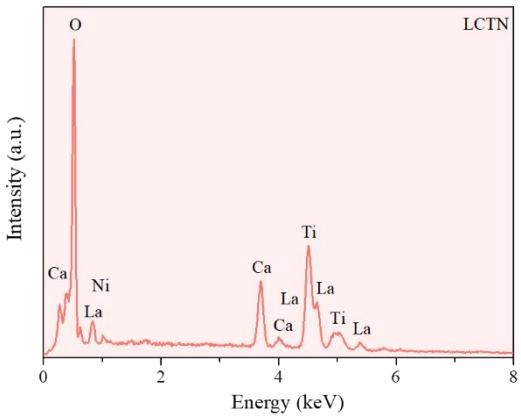

Figure S11. EDX pattern of the LCTN.

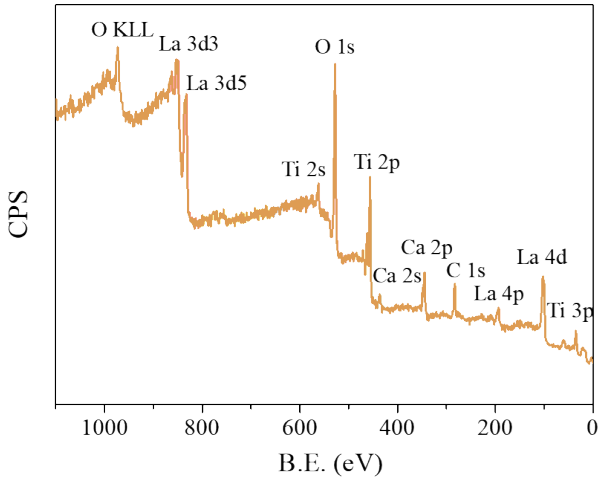

Figure S12. Full XPS spectrum of LCT.

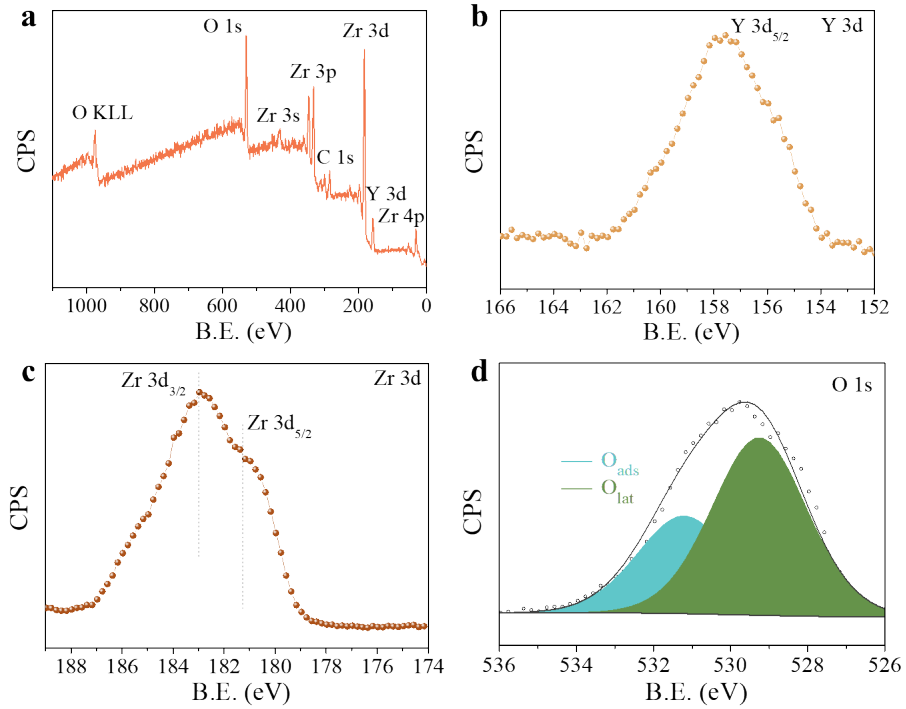

Figure S13. **a,** Full XPS spectrum of YSZ. **b,** EDX pattern of the LCTN. XPS spectra of (**b)** Y 3d, (**c)** Zr 3d and (**d)** O 1s of the YSZ.

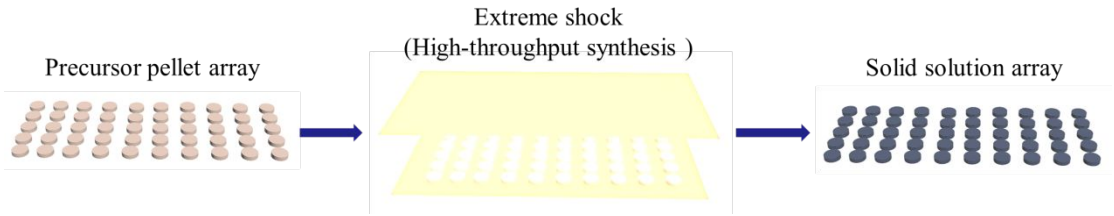

Figure S14. Schematic of the high-throughput synthesis of functional ceramic materials by thermal shock technique.

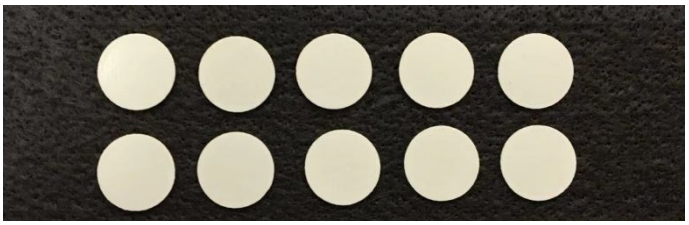

Figure S15. Picture of preparation of multiple samples using thermal shock.

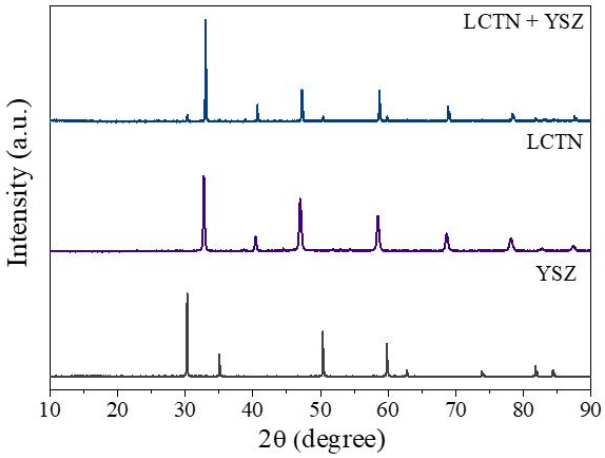

Figure S16. XRD profile of LCTN electrode on the YSZ electrolyte after sintering at 1200 ℃ for 3 h. For comparison, XRD profiles of LCTN and YSZ are also shown.

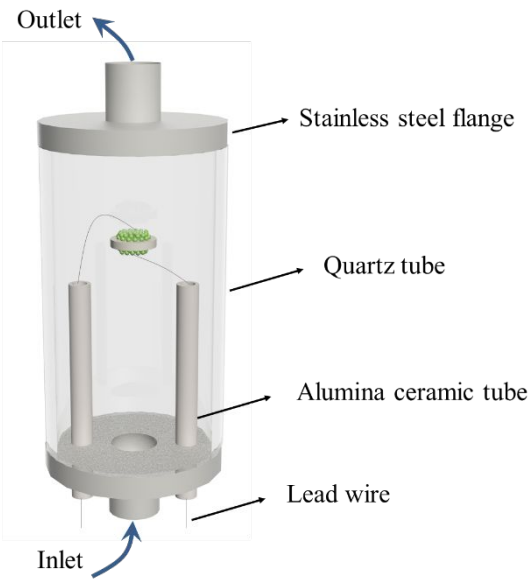

Figure S17. Schematic of the home-made setup for the electrochemical experiments.

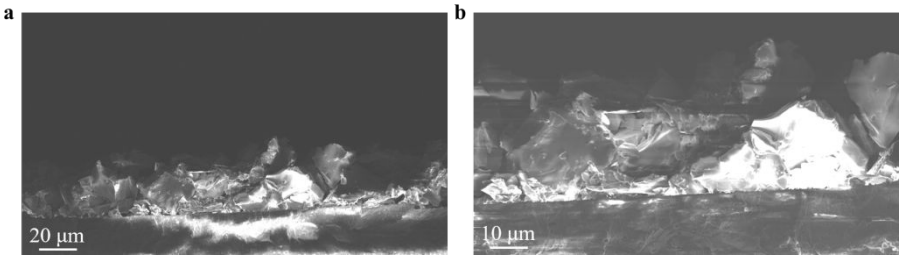

Figure S18. SEM images of the cross-section view of the conventional LCT.

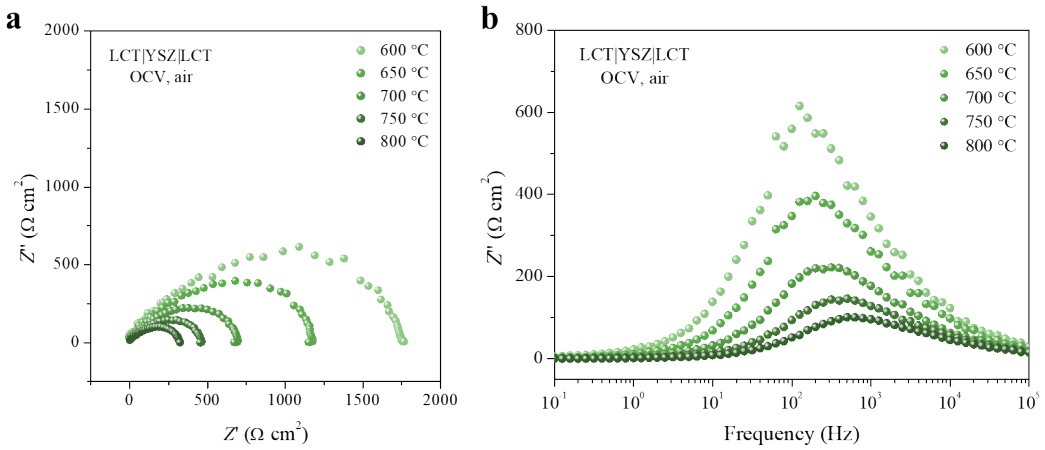

Figure S19. **(a)** Nyquist and **(b)** Bode plots of the YSZ electrolyte-supported symmetrical cell with conventional furnace synthesized LCT as electrode collected from 600 to 800 ℃ in air under OCV conditions.

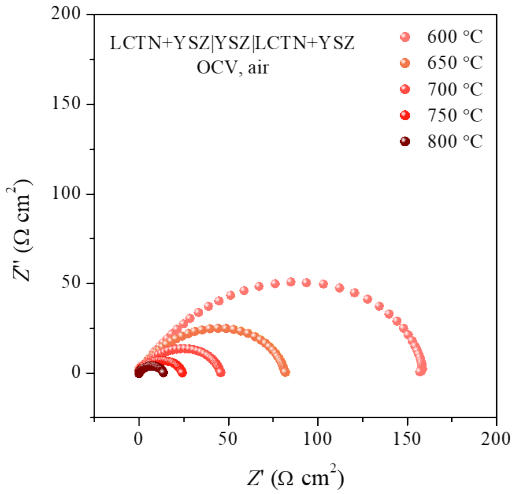

Figure S20. Nyquist plots of the LCTN:YSZ(50:50)|YSZ|LCTN:YSZ(50:50) symmetrical cell collected from 600 to 800 ℃ in air under OCV conditions.

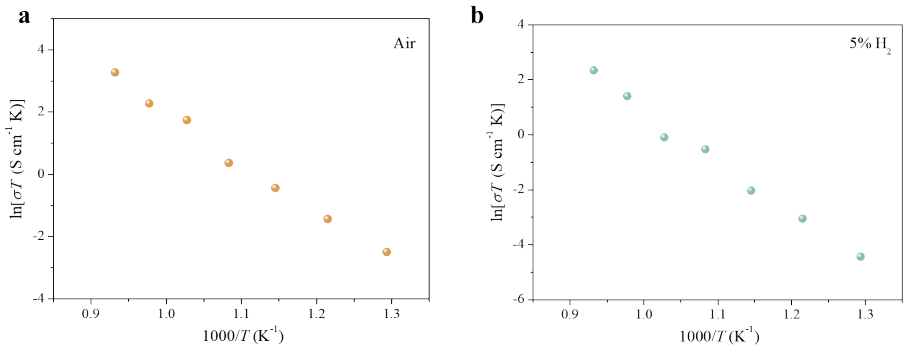

Figure S21. Conductivity as a function of temperature for LCTN measured in air and 5%H_2 atmospheres.

Table S1. Refined structural parameters for YSZ obtained by fitting of powder XRD data at room temperature.

Atoms, sites	Parameters	YSZ
	Space group	Fm-3m (225)
	a (Å)	5.1411 (1)
	b (Å)	5.1411 (1)
	c (Å)	5.1411 (1)
	V (Å^3)	135.88
Y, 4a	x	0
	y	0
	z	0
	Occupancy	0.14
Zr, 4a	x	0
	y	0
	z	0
	Occupancy	0.82
O, 8c	x	0.25
	y	0.25
	z	0.25
	Occupancy	0.93
	R_{wp}	7.25
	R_p	5.81
	χ^2	3.89

Table S2. Refined structural parameters for SDC obtained by fitting of powder XRD data at room temperature.

Atoms, sites	Parameters	SDC
	Space group	Fm-3m (225)
	a (Å)	5.4176 (4)
	b (Å)	5.4176 (4)
	c (Å)	5.4176 (4)
	V (Å^3)	159.01
Sm, 4a	x	0
	y	0
	z	0
	Occupancy	0.2
Ce, 4a	x	0
	y	0
	z	0
	Occupancy	0.8
O, 8c	x	0.25
	y	0.25
	z	0.25
	Occupancy	0.95
	R_{wp}	18.47
	R_p	16.02
	χ^2	14.91

Table S3. Refined structural parameters for LCT obtained by fitting of powder XRD data at room temperature.

Atoms, sites	Parameters	LCT
	Space group	Pbnm (62)
	a (Å)	5.4638 (6)
	b (Å)	7.7173 (5)
	c (Å)	5.4688 (9)
	V (Å^3)	230.60
La, 4c	x	0.4670
	y	0.2500
	z	0.0072
	Occupancy	0.4
Ca, 4c	x	0.4670
	y	0.2500
	z	0.0072
	Occupancy	0.4
Ti, 4a	x	0
	y	0
	z	0
	Occupancy	1
O1, 4c	x	0.5107
	y	0.2500
	z	0.5722
	Occupancy	1
O1, 8d	x	0.2158
	y	0.0346
	z	0.2826
	Occupancy	1
	R_{wp}	10.97
	R_p	7.25
	χ^2	3.87

Table S4. Refined structural parameters for LCTN obtained by fitting of powder XRD data at room temperature.

Atoms, sites	Parameters	LCTN
	Space group	Pbnm (62)
	a (Å)	5.4698 (7)
	b (Å)	7.7372 (8)
	c (Å)	5.4636 (7)
	V (Å^3)	231.22
La, 4c	x	0.4670
	y	0.2500
	z	0.0072
	Occupancy	0.4
Ca, 4c	x	0.4670
	y	0.2500
	z	0.0072
	Occupancy	0.4
Ti, 4a	x	0
	y	0
	z	0
	Occupancy	0.94
Ni, 4a	x	0
	y	0
	z	0
	Occupancy	0.06
O1, 4c	x	0.5107
	y	0.2500
	z	0.5722
	Occupancy	1
O1, 8d	x	0.2158
	y	0.0346
	z	0.2826
	Occupancy	1
	R_{wp}	17.67
	R_p	12.65
	χ^2	8.42

Table S5. Refined structural parameters for STO obtained by fitting of powder XRD data at room temperature.

Atoms, sites	Parameters	STO
	Space group	Pm-3m (221)
	a (Å)	3.9064 (5)
	b (Å)	3.9064 (5)
	c (Å)	3.9064 (5)
	V (Å^3)	59.61
Sr, 1b	x	0.5
	y	0.5
	z	0.5
	Occupancy	1
Ti, 1a	x	0
	y	0
	z	0
	Occupancy	1
O, 3d	x	0.5
	y	0
	z	0
	Occupancy	1
	R_{wp}	12.10
	R_p	9.65
	χ^2	22.96

Table S6. Parameters customized for different materials during the thermal shock.

Samples	Carbon felt dimension (L*W, cm)	Current (A)	Current density (A cm^{-2})	Shocking time (s)
LCT	8*1.5	19	1.6	60
LCTN	8*1.5	19	1.6	55
STO	8*1.5	19	1.6	70
YSZ	8*1.5	20	1.7	150
SDC	8*1.5	20	1.7	80